PHASE DIAGRAMS

H. P. R. Frederikse

A phase is a structurally homogeneous portion of matter. Regardless of the number of chemical constituents of a gas, there is only one vapor phase. This is true also for the liquid form of a pure substance, although a mixture of several liquid substances may exist as one or several phases, depending on the interactions among the substances. On the other hand a pure solid may exist in several phases at different temperatures and pressures because of differences in crystal structure (Reference 1). At the phase transition temperature, T_{tr}, the chemical composition of the solid remains the same, but often a change in the physical properties will take place. Such changes are found in ferroelectric crystals (example $BaTiO_3$) which develop a spontaneous polarization below T_{tr}, in superconductors (example Pb) which loose all electrical resistance below the transition point, and in many other classes of solids.

In quite a few cases it is difficult to bring about the phase transition, and the high- (or low-) temperature phase persists in its metastable form. Many liquids remain in the liquid state for shorter or longer periods of time when cooled below the melting point (supercooling). However, often the slightest disturbance will cause solidification. Persistence of the high temperature phase in solid-solid transitions is usually of much longer duration. An example of this behavior is found in white tin; although gray tin is the thermodynamically stable form below T_{tr} (286.4 K), the metal remains in its undercooled, white tin state all the way to T = 0 K, and crystals of gray tin are very difficult to produce.

A *phase diagram* is a map which indicates the areas of stability of the various phases as a function of external conditions (temperature and pressure). Pure materials, such as mercury, helium, water, and methyl alcohol are considered one-component systems and they have *unary* phase diagrams. The equilibrium phases in two-component systems are presented in *binary* phase diagrams. Because many important materials consist of three, four, and more components, many attempts have been made to deduce their multicomponent phase diagrams. However, the vast majority of systems with three or more components are very complex, and no overall maps of the phase relationships have been worked out.

It has been shown during the last 20 to 25 years that very useful partial phase diagrams of complex systems can be obtained by means of thermodynamic modeling (References 2, 3). Especially for complicated, multicomponent alloy systems the CALPHAD method has proved to be a successful approach for producing valuable portions of very intricate phase diagrams (Reference 4). With this method thermodynamic descriptions of the free energy functions of various phases are obtained which are consistent with existing (binary) phase diagram information and other thermodynamic data. Extrapolation methods are then used to extend the thermodynamic functions into a ternary system. Comparison of the results of this procedure with available experimental data is then used to fine-tune the phase diagram and add ternary interaction functions if necessary. In principle this approximation strategy can be extended to four, five, and more component systems.

The nearly two dozen phase diagrams shown below present the reader with examples of some important types of single and multicomponent systems, especially for ceramics and metal alloys. This makes it possible to draw attention to certain features like the kinetic aspects of phase transitions (see Figure 22, which presents a time-temperature-transformation, or TTT, diagram for the precipitation of α-phase particles from the β-phase in a Ti-Mo alloy; Reference 1, pp. 358–360). The general references listed below and the references to individual figures contain phase diagrams for many additional systems.

General References

1. Ralls, K. M., Courtney, T. H., and Wulff, J., *Introduction to Materials Science and Engineering*, Chapters 16 and 17, John Wiley & Sons, New York, 1976.
2. Kaufman, L., and Bernstein, H., *Computer Calculation of Phase Diagrams*, Academic Press, New York, 1970.
3. Kattner, U. R., Boettinger, W. J. B., and Coriell, S. R., *Z. Metallkd.*, 87, 9, 1996.
4. Dinsdale, A. T., Ed., *CALPHAD*, Vol. 1–20, Pergamon Press, Oxford, 1977–1996 and continuing.
5. Baker, H., Ed., *ASM Handbook, Volume 3: Alloy Phase Diagrams*, ASM International, Materials Park, OH, 1992.
6. Massalski, T. B., Ed., *Binary Alloy Phase Diagrams, Second Edition*, ASM International, Materials Park, OH, 1990.
7. Roth. R. S., Ed., *Phase Diagrams for Ceramists*, Vol. I (1964) to Volume XI (1995), American Ceramic Society, Waterville, OH.

References to Individual Phase Diagrams

Figure 1. Carbon: Reference 7, Vol. X (1994), Figure 8930. Reprinted with permission.
Figure 2. Si-Ge : Ref.5, p. 2.231. Reprinted with permission.
Figure 3. H_2O (ice): See figure.
Figure 4. SiO_2: Reference 7, Vol. XI (1995), Figure 9174. Reprinted with permission.
Figure 5. Fe-O: Darken, L.S., and Gurry, R.W., *J. Am. Chem. Soc.*, 68, 798, 1946. Reprinted with permission.
Figure 6. Ti-O: Reference 5, p. 2.324. Reprinted with permission.
Figure 7. BaO-TiO_2: Reference 7, Vol. III (1975), Figure 4302. Reprinted with permission.
Figure 8. MgO-Al_2O_3: Reference 7, Vol. XI (1995), Figure 9239. Reprinted with permission.
Figure 9. Y_2O_3-ZrO_2: Reference 7, Vol. XI (1995), Figure 9348. Reprinted with permission.
Figure 10. Si-N-Al-O (Sialon): Reference 7, Vol. X (1994), Figure 8759. Reprinted with permission.
Figure 11. PbO-ZrO_2-TiO_2 (PZT): Reference 7, Vol. III (1975), Figure 4587. Reprinted with permission.
Figure 12. Al-Si-Ca-O: Reference 7 (1964), Vol. I, Figure 630. Reprinted with permission.
Figure 13. Y-Ba-Cu-O: Whitler, J.D., and Roth, R.S., *Phase Diagrams for High T_c Superconductors*, Figure S-082, American Ceramic Society, Waterville, OH, 1990. Reprinted with permission.
Figure 14. Al-Cu: Reference 5, p. 2.44. Reprinted with permission.
Figure 15. Fe-C: Ralls, K.M., Courtney, T.H., and Wulff, J., *Introduction to Materials Science and Engineering*, Figure 16.13 , John Wiley & Sons, New York, 1976. Reprinted with permission.
Figure 16. Fe-Cr: Reference 5, p. 2.152. Reprinted with permission.
Figure 17. Cu-Sn: Reference 5, p. 2.178. Reprinted with permission.
Figure 18. Cu-Ni: Reference 5, p. 2.173. Reprinted with permission.
Figure 19. Pb-Sn (solder): Reference 5, p. 2.335. Reprinted with permission.
Figure 20. Cu-Zn (brass): Subramanian, P.R., Chakrabarti, D.J., and Laughlin, D.E., Editors, *Phase Diagrams of Binary Copper Alloys*, p. 487, ASM International, Materials Park, OH, 1994. Reprinted with permission.
Figure 21. Co-Sm: Reference 5, p. 2.148. Reprinted with permission.
Figure 22. Ti-Mo: Reference 5, p. 2.296; Reference 1, p. 359. Reprinted with permission.
Figure 23: Fe-Cr-Ni: Reference 5, Figure 48. Reprinted with permission.

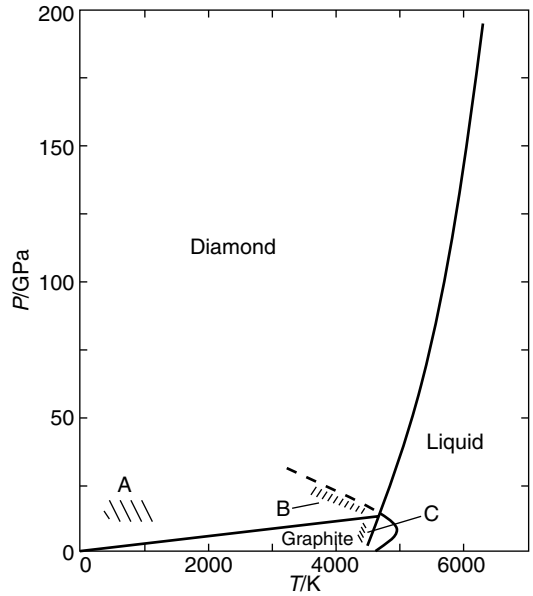

FIGURE 1. Phase diagram of carbon. (A) Martensitic transition: hex graphite → hex diamond. (B) Fast graphite-to-diamond transition. (C) Fast diamond-to-graphite transition.

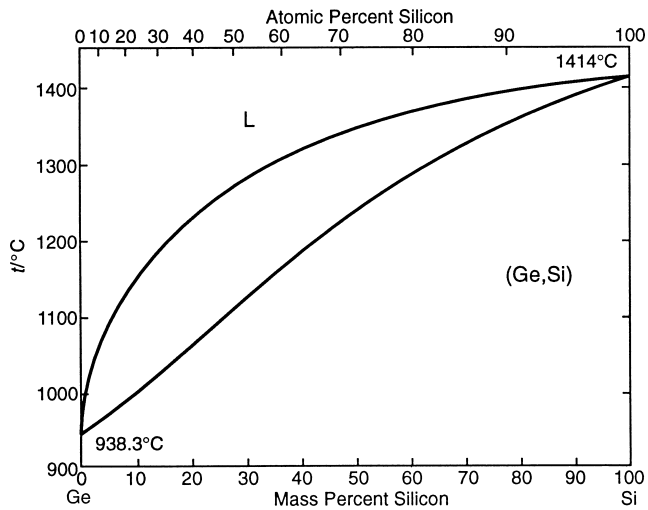

FIGURE 2. Si-Ge system.

Phase	Composition, mass % Si	Pearson symbol	Space group
(Ge,Si)	0 to 100	*cF*8	$Fd\bar{3}m$
High-pressure phases			
GeII	–	*tI*4	$I4_1/amd$
SiII	–	*tI*4	$I4_1/amd$

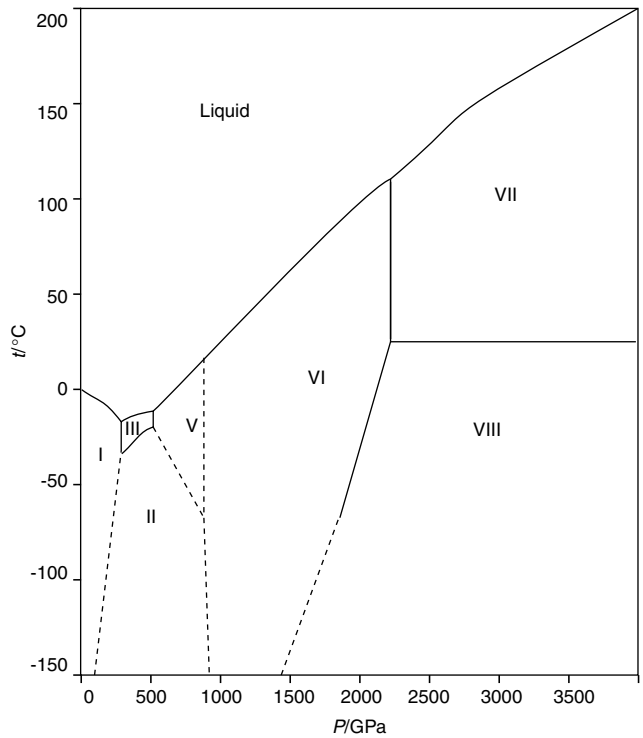

FIGURE 3. Diagram of the principal phases of ice. Solid lines are measured boundaries between stable phases; dotted lines are extrapolated. Ice IV is a metastable phase which exists in the region of ice V. Ice IX exists in the region below –100°C and pressures in the range 200–400 MPa. Ice X exists at pressures above 44 GPa. See Table 1 for the coordinates of the triple points, where liquid water is in equilibrium with two adjacent solid phases.

TABLE 1. Crystal Structure, Density, and Transition Temperatures for the Phases of Ice

Phase	Crystal system	Cell parameters	Z	n	ρ/g cm^{-3}	Triple ponts
Ih	Hexagonal	a = 4.513; c = 7352	4	4	0.93	I-III: –21.99°C, 209.9 MPa
Ic	Cubic	a = 6.35	8	4	0.94	
II	Rhombohedral	a = 7.78; α = 113.1°	12	4	1.18	
III	Tetragonal	a = 6.73; c = 6.83	12	4	1.15	III-V: –16.99°C, 350.1 MPa
IV	Rhombohedral	a = 7.60; α = 70.1°	16	4	1.27	
V	Monoclinic	a = 9.22; b = 7.54, c = 10.35; β = 109.2°	28	4	1.24	V-VI: 0.16°C, 632.4 MPa
VI	Tetragonal	a = 6.27; c = 5.79	10	4	1.31	VI-VII: 82°C, 2216 MPa
VII	Cubic	a = 3.41	2	8	1.56	
VIII	Tetragonal	a = 4.80; c = 6.99	8	8	1.56	
IX	Tetragonal	a = 6.73; c = 6.83	12	4	1.16	
X	Cubic	a = 2.83	2	8	2.51	

References

1. Wagner, W., Saul, A., and Pruss, A., *J. Phys. Chem. Ref. Data*, 23, 515, 1994.
2. Lerner, R.G. and Trigg, G.L., Eds., *Encyclopedia of Physics,* VCH Publishers, New York, 1990.
3. Donnay, J.D.H. and Ondik, H.M, *Crystal Data Determinative Tables, Third Edition, Volume 2, Inorganic Compounds,* Joint Committee on Powder Diffraction Standards, Swarthmore, PA, 1973.
4. Hobbs, P.V., *Ice Physics,* Oxford University Press, Oxford, 1974.
5. Glasser, L., *J. Chem. Edu.,* 81, 414, 2004.

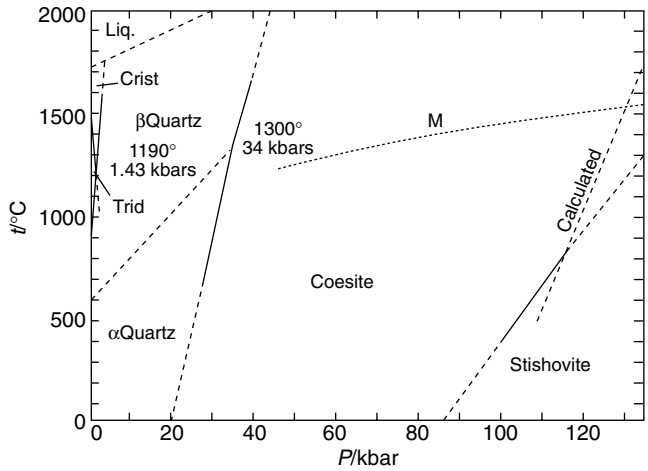

FIGURE 4. SiO_2 system. Crist = cristobalite; Trid = tridymite.

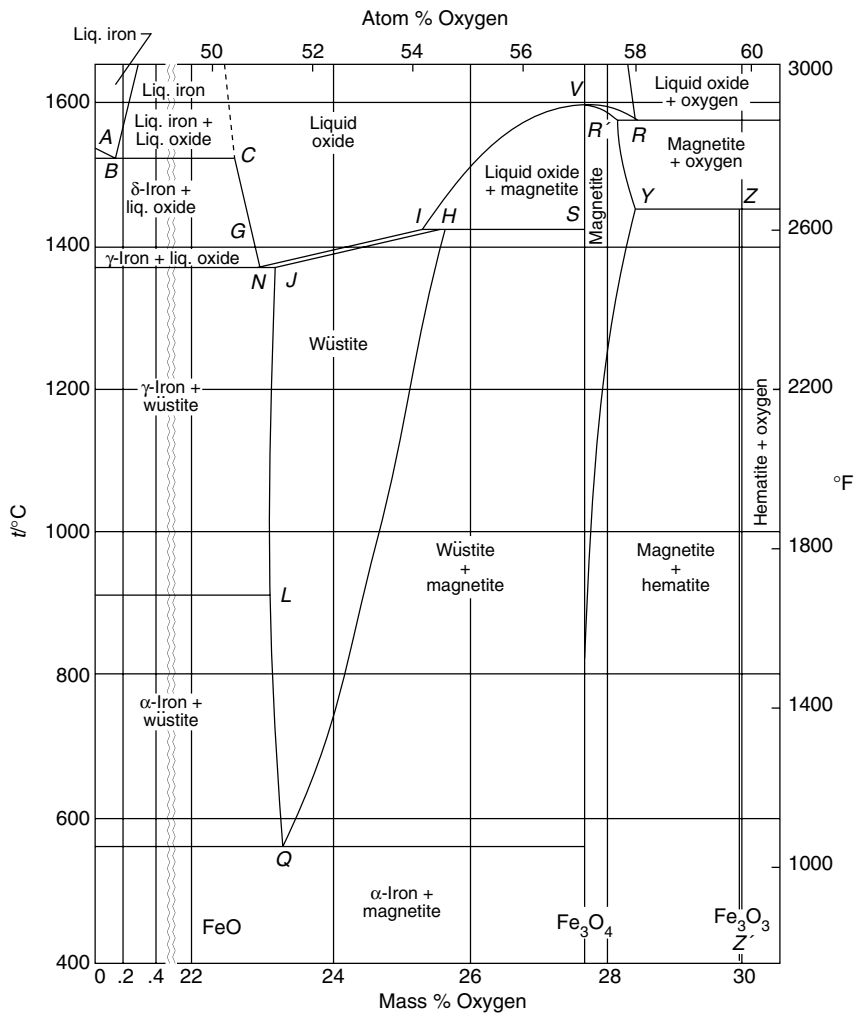

FIGURE 5. Fe-O system.

Point	t/°C	% O	p_{CO_2}/p_{CO}	Point	t/°C	% O	p_{CO_2}/p_{CO}	p_{O_2}/atm
A	1539			*Q*	560	23.26	1.05	
B	1528	0.16	0.209	*R*	1583	28.30		1
C	1528	22.60	0.209	*R′*	1583	28.07		1
G	1400[a]	22.84	0.263	*S*	1424	27.64	16.2	
H	1424	25.60	16.2	*V*	1597	27.64		0.0575
I	1424	25.31	16.2	*Y*	1457	28.36		1
J	1371	23.16	0.282	*Z*	1457	30.04		1
L	911[a]	23.10	0.447	*Z′*		30.6		
N	1371	22.91	0.282					

[a] Values for pure iron.

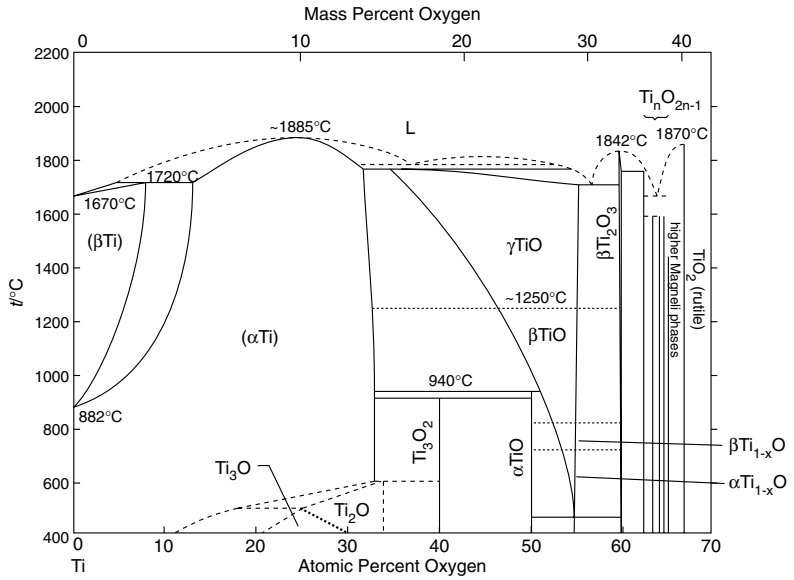

FIGURE 6. Ti-O system.

Phase	Composition, mass % O	Pearson symbol	Space group
(βTi)	0 to 3	*cI*2	$Im\bar{3}m$
(αTi)	0 to 13.5	*hP*2	$P63/mmc$
Ti_3O	~8 to ~13	*hP*~16	$P\bar{3}c$
Ti_2O	~10 to 14.4	*hP*3	$P\bar{3}m1$
γTiO	15.2 to 29.4	*cF*8	$Fm\bar{3}m$
Ti_3O_2	~18	*hP*~5	$P6/mmm$
βTiO	~24 to ~29.4	*c***	–
αTiO	~25.0	*mC*16	$A2/m$ or $B^*/^*$
$\beta Ti_{1-x}O$	~29.5	*oI*12	$I222$
$\alpha Ti_{1-x}O$	~29.5	*tI*18	$I4/m$
βTi_2O_3	33.2 to 33.6	*hR*30	$R\bar{3}c$
αTi_2O_3	33.2 to 33.6	*hR*30	$R\bar{3}c$
βTi_3O_5	35.8	*m***	–
αTi_3O_5	35.8	*mC*32	$C2/m$
$\alpha' Ti_3O_5$	35.8	*mC*32	Cc
γTi_4O_7	36.9	*aP*44	$P\bar{1}$
βTi_4O_7	36.9	*aP*44	$P\bar{1}$
$\alpha Ti4O_7$	36.9	*aP*44	$P\bar{1}$
γTi_5O_9	37.6	*aP*28	$P\bar{1}$
βTi_6O_{11}	38.0	*aC*68	$A\bar{1}$
Ti_7O_{13}	38.3	*aP*40	$P\bar{1}$
Ti_8O_{15}	38.5	*aC*92	$A\bar{1}$
Ti_9O_{17}	38.7	*aP*52	$P\bar{1}$
Rutile TiO_2	40.1	*tP*6	$P4_2/mnm$
Metastable phases			
Anatase	–	*tI*12	$I4_1/amd$
Brookite	–	*oP*24	$Pbca$
High-pressure phases			
TiO_2-II	–	*oP*12	$Pbcn$
TiO_2-III	–	*hP*~48	–

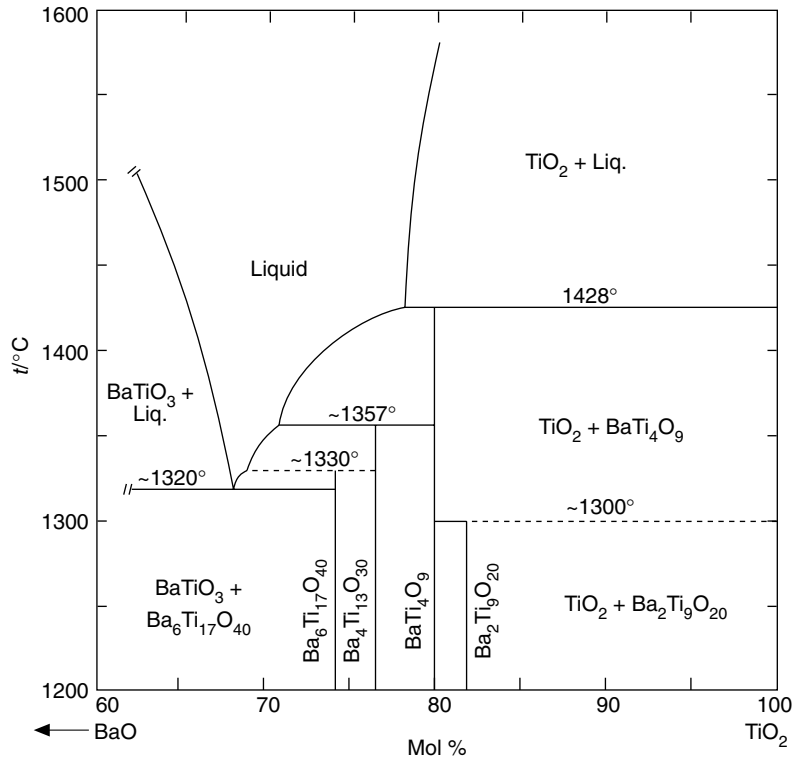

FIGURE 7. $BaO\text{-}TiO_2$ system.

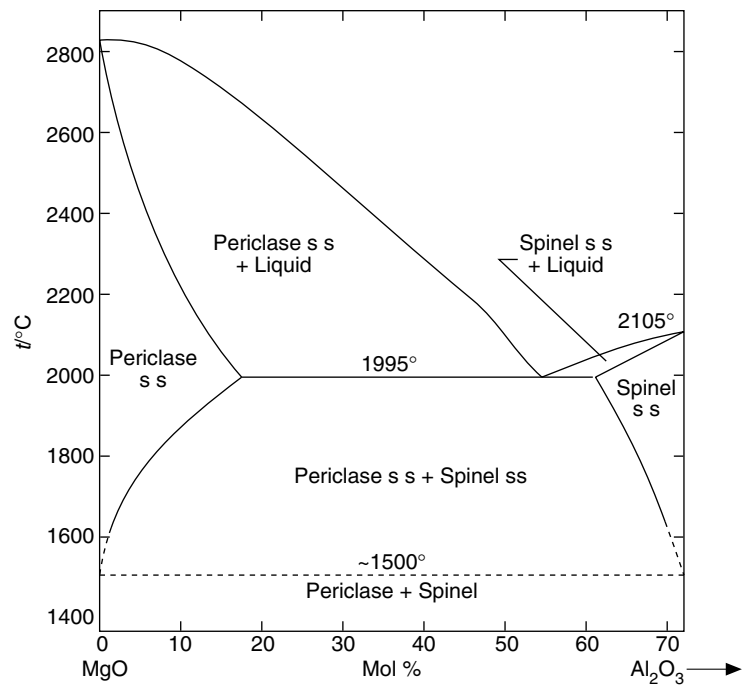

FIGURE 8. $MgO\text{-}Al_2O_3$ system.

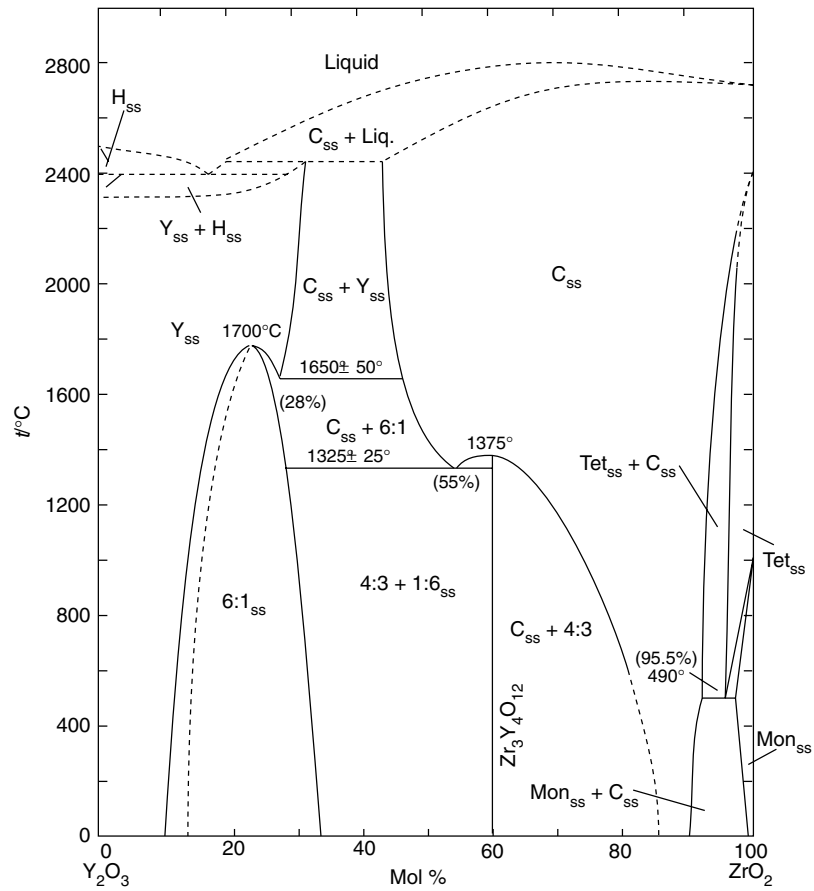

FIGURE 9. Y_2O_3-ZrO_2 system. C_{ss} = cubic ZrO_2 ss (fluorite-type ss); Y_{ss} = cubic Y_2O_3 ss; Tet_{ss} = tetragonal ZrO_2 ss; Mon_{ss} = monoclinic ZrO_2 ss; H_{ss} = hexagonal Y_2O_3 ss; 3:4 = $Zr_3Y_4O_{12}$; 1:6 = ZrY_6O_{11} ss.

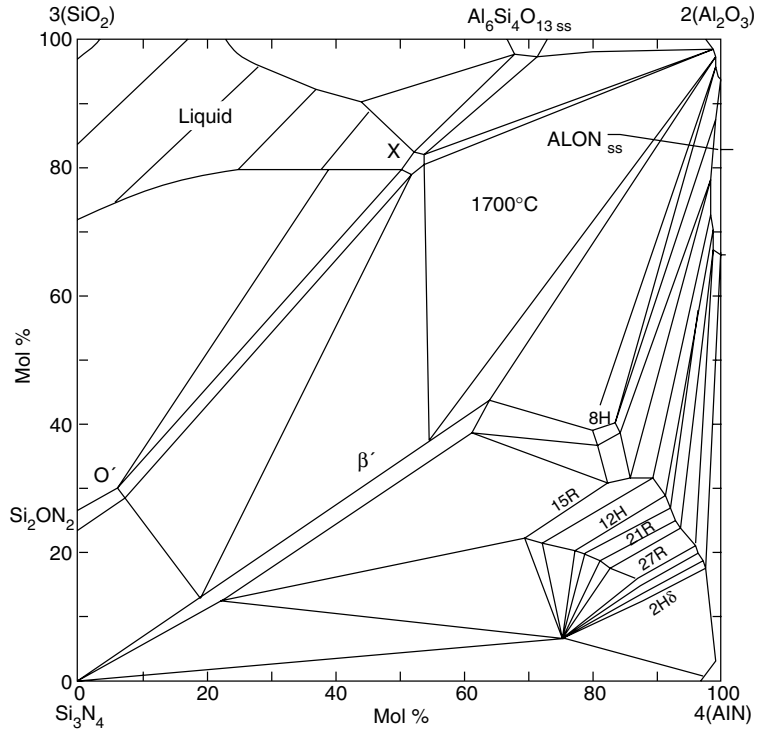

FIGURE 10. $3(SiO_2)$-Si_3N_4-$4(AlN)$-$2(Al_2O_3)$ system. "Behavior" diagram at 1700°C. The labels 8H, 15R, 12H, 21R, 27R, $2H^{\delta}$ indicate defect AlN polytypes. β´ = 3-sialon ($Si_{6-x}Al_xO_xN_{8-x}$); O´ = sialon of Si_2ON_2 type; X = $SiAlO_2N$ ("nitrogen mullite"). ALON ss = aluminum oxynitride ss extending from approximately Al_7O_9N to Al_3O_3N.

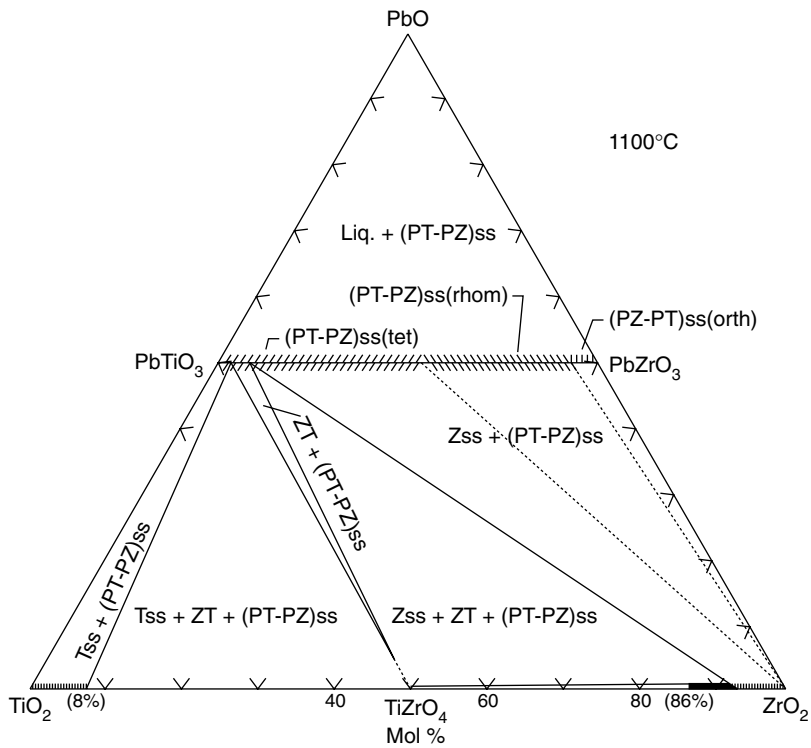

FIGURE 11. PbO-ZrO_2-TiO_2 (PZT) system, subsolidus at 1100°C. P = PbO; T = TiO_2; Z = ZrO_2.

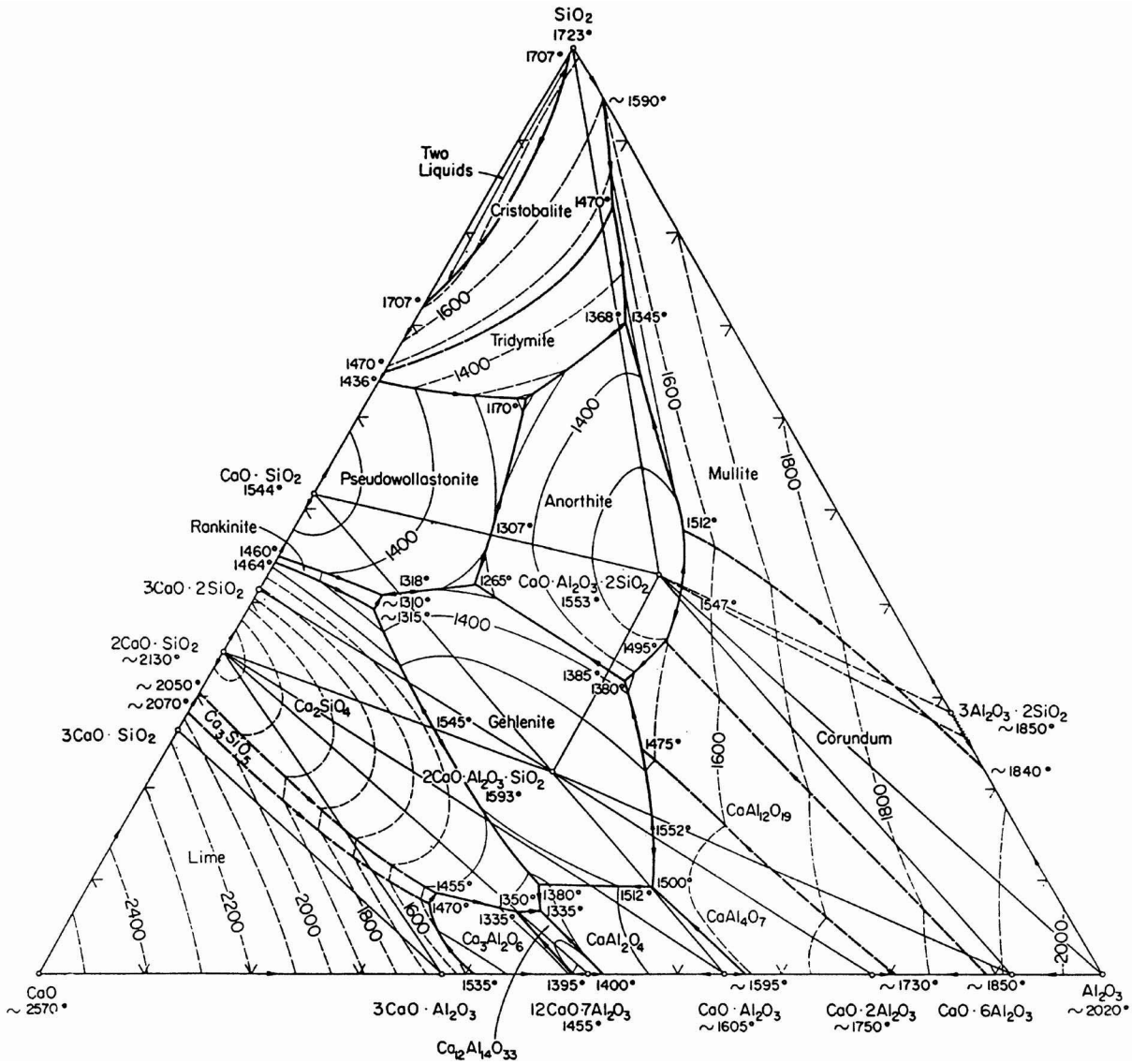

FIGURE 12. CaO-Al_2O_3-SiO_2 system (temperatures in °C).

Crystalline Phases

Notation	Oxide formula
Cristobalite, Tridymite	SiO_2
Pseudowollastonite	$CaO{\cdot}SiO_2$
Rankinite	$3CaO{\cdot}2SiO_2$
Lime	CaO
Corundum	Al_2O_3
Mullite	$3Al_2O_3{\cdot}2SiO_2$
Anorthite	$CaO{\cdot}Al_2O_3{\cdot}2SiO_2$
Gehlenite	$2CaO{\cdot}Al_2O_3{\cdot}SiO_2$

Temperatures up to approximately 1550°C are on the Geophysical Laboratory Scale; those above 1550°C are on the 1948 International Scale.

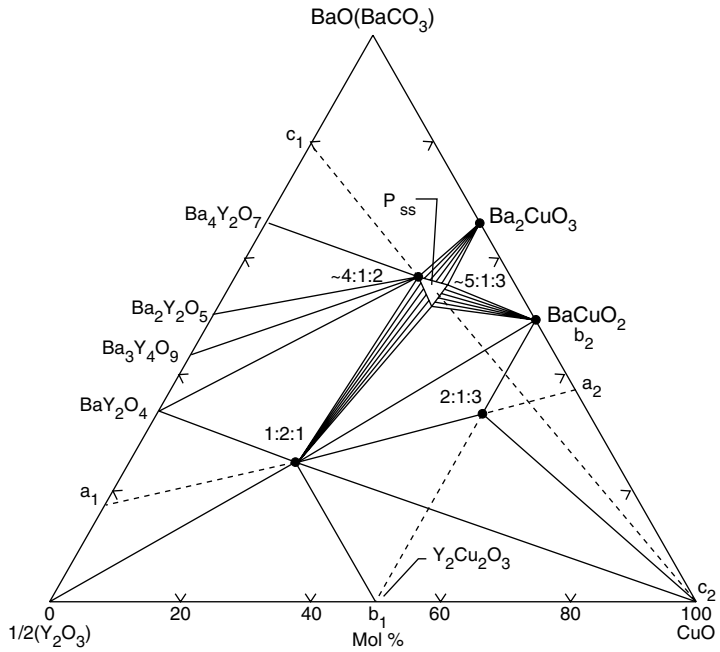

FIGURE 13. BaO-Y_2O_3-CuO system. 2:1:3 = $Ba_2YCu_3O_{7-x}$; 1:2:1 = BaY_2CuO_5; 4:1:2 = $Ba_4YCu_2O_{7.5+x}$; and 5:1:3 = $Ba_5YCu_3O_{9.5+x}$. The superconducting 2:1:3 phase was prepared using barium peroxide.

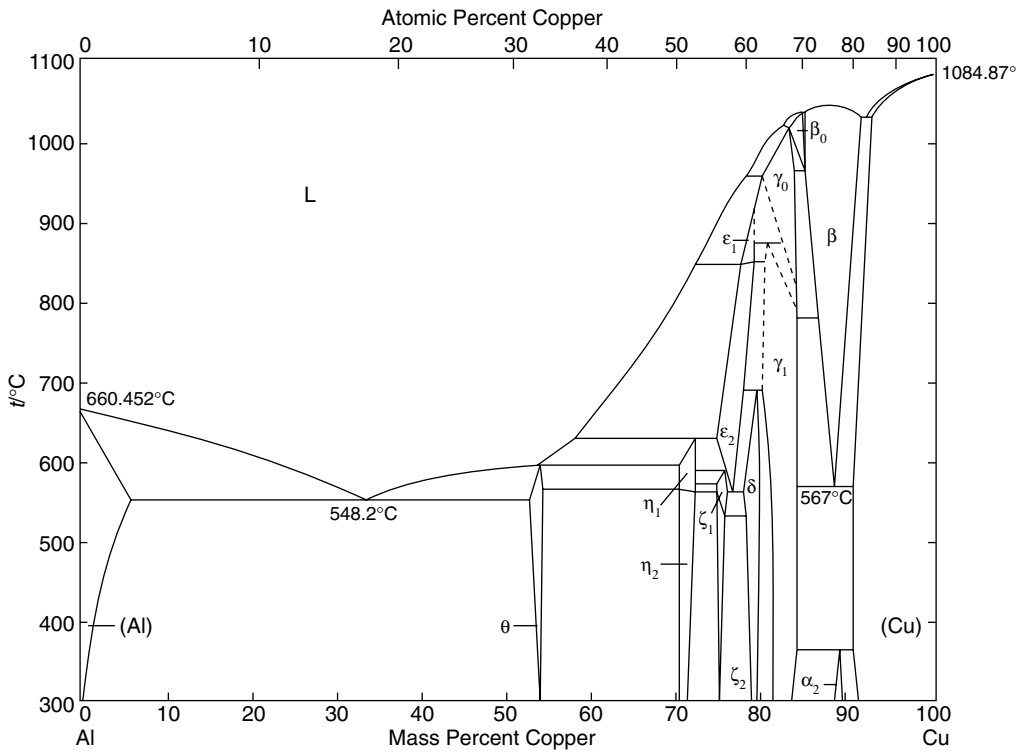

FIGURE 14. Al-Cu system.

Phase	Composition, wt % Cu	Pearson symbol	Space group
(Al)	0 to 5.65	*cF*4	$Fm\bar{3}m$
θ	52.5 to 53.7	*tI*12	*I*4/*mcm*
η_1	70.0 to 72.2	*oP*16 or *oC*16	*Pban* or *Cmmm*
η_2	70.0 to 72.1	*mC*20	*C*2/*m*
ζ_1	74.4 to 77.8	*hP*42	*P*6/*mmm*
ζ_2	74.4 to 75.2	(a)	–
ε_1	77.5 to 79.4	(b)	–
ε_2	72.2 to 78.7	*hP*4	*P*63/*mmc*
δ	77.4 to 78.3	(c)	$R\bar{3}m$
γ_0	77.8 to 84	(d)	–
γ_1	79.7 to 84	*cP*52	$P\bar{4}3m$
β_0	83.1 to 84.7	(d)	–
β	85.0 to 91.5	*cI*2	$Im\bar{3}m$
α_2	88.5 to 89	(e)	–
(Cu)	90.6 to 100	*cF*4	$Fm\bar{3}m$
Metastable phases			
θ′	–	*tP*6	–
β′	–	*cF*16	$Fm\bar{3}m$
Al_3Cu_2	61 to 70	*hp*5	$P\bar{3}m1$

(a) Monoclinic? (b) Cubic? (c) Rhombohedral. (d) Unknown. (e) $D0_{22}$-type long-period superlattice.

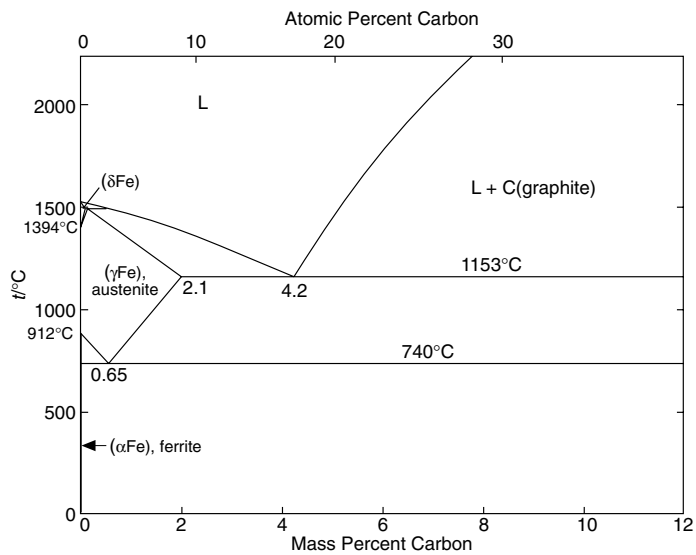

FIGURE 15. Fe-C system.

Phase	Composition, mass % C	Pearson symbol	Space group
(δFe)	0 to 0.09	*cI*2	$Im\bar{3}m$
(γFe)	0 to 2.1	*cF*4	$Fm\bar{3}m$
(αFe)	0 to 0.021	*cI*2	$Im\bar{3}m$
(C)	100	*hP*4	$P6_3/mmc$
Metastable/high-pressure phases			
(εFe)	0	*hP*2	$P6_3/mmc$
Martensite	< 2.1	*tI*4	*I*4/*mmm*
Fe_4C	5.1	*cP*5	$P\bar{4}3m$
Fe_3C (θ)	6.7	*oP*16	*Pnma*
Fe_5C_2 (χ)	7.9	*mC*28	*C*2/*c*
Fe_7C_3	8.4	*hP*20	$P6_3mc$
Fe_7C_3	8.4	*oP*40	*Pnma*
Fe_2C (η)	9.7	*oP*6	*Pnnm*
Fe_2C (ε)	9.7	*hP**	$P6_322$
Fe_2C	9.7	*hP**	$P\bar{3}m1$
(C)	100	*cF*8	$Fd\bar{3}m$

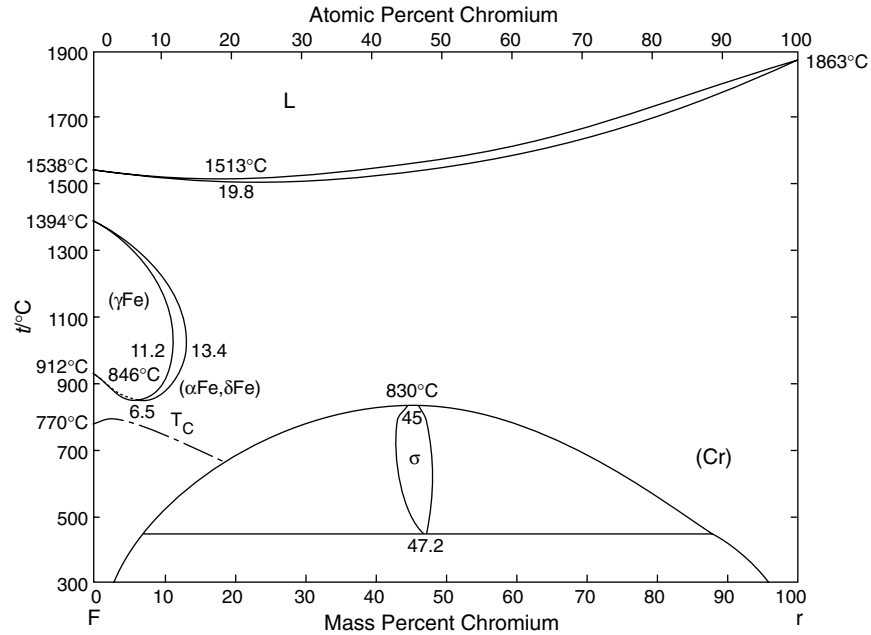

FIGURE 16. Fe-Cr system.

Phase	Composition, mass % Cr	Pearson symbol	Space group
(aFe, Cr)	0 to 100	*cI*2	$Im\bar{3}m$
(γFe)	0 to 11.2	*cF*4	$Fm\bar{3}m$
σ	42.7 to 48.2	*tP*30	$P4_2/mnm$

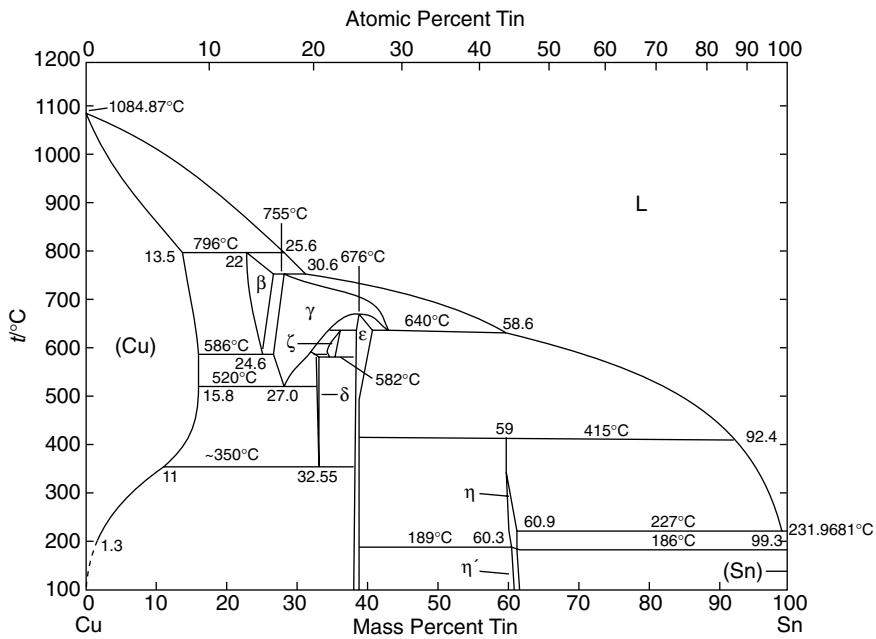

FIGURE 17. Cu-Sn system.

Phase	Composition, mass % Sn	Pearson symbol	Space group
α	0 to 15.8	*cF*4	$Fm\bar{3}m$
β	22.0 to 27.0	*cI*2	$Im\bar{3}m$
γ	25.5 to 41.5	*cF*16	$Fm\bar{3}m$
δ	32 to 33	*cF*416	$F\bar{4}3m$
ζ	32.2 to 35.2	*hP*26	$P6_3$
ε	27.7 to 39.5	*oC*80	*Cmcm*
η	59.0 to 60.9	*hP*4	$P6_3/mmc$
η´	44.8 to 60.9	(a)	–
(βSn)	~100	*tI*4	$I4_1/amd$
(αSn)	100	*cF*8	$Fd\bar{3}m$

(a) Hexagonal; superlattice based on NiAs-type structure.

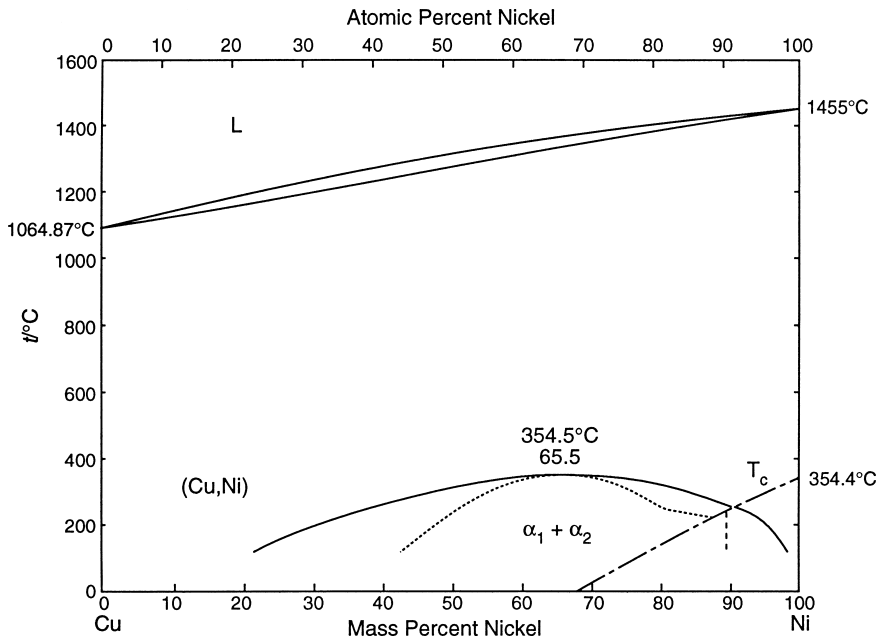

FIGURE 18. Cu-Ni system.

Phase	Composition, mass % Ni	Pearson symbol	Space group
(Cu, Ni) (above 354.5°C)	0 to 100	*cF*4	$Fm\bar{3}m$

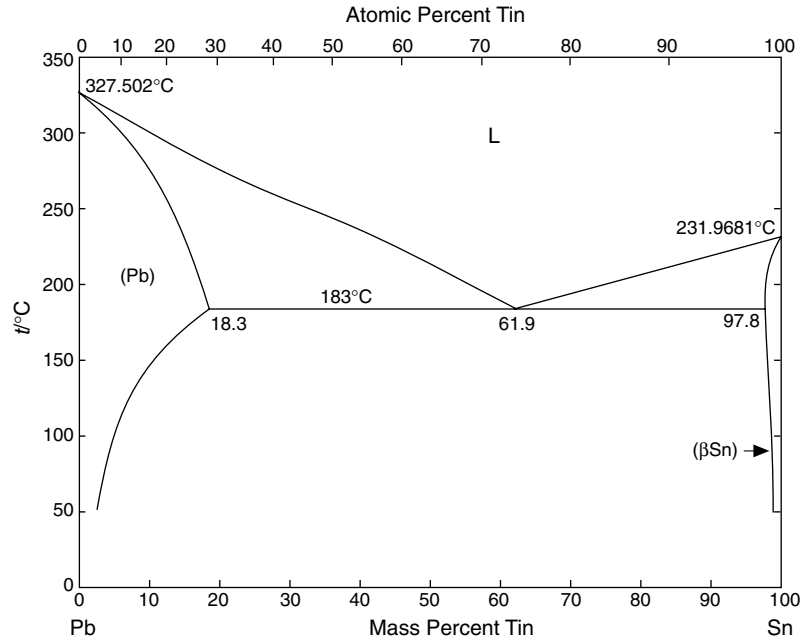

FIGURE 19. Pb-Sn system.

Phase	Composition, mass % Sn	Pearson symbol	Space group
(Pb)	0 to 18.3	*cF*4	$Fm\bar{3}m$
(βSn)	97.8 to 100	*tI*4	$I4_1/amd$
(αSn)	100	*cF*8	$Fd\bar{3}m$
High-pressure phases			
ε(a)	52 to 74	*hP*1	*P*6/*mmm*
ε´(b)	52	*hP*2	$P6_3/mmc$

(a) From phase diagram calculated at 2500 MPa. (b) This phase was claimed for alloys at 350°C and 5500 MPa.

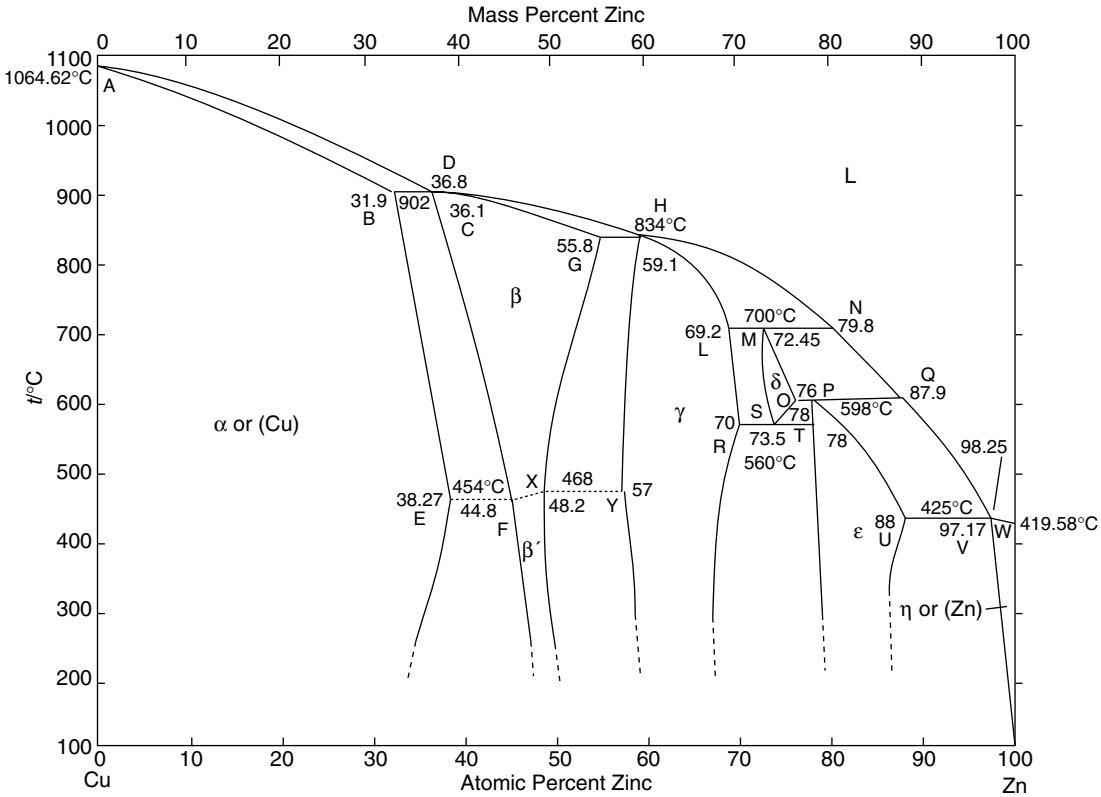

FIGURE 20. Cu-Zn system.

Phase	Composition, mass % Zn	Pearson symbol	Space group
α or (Cu)	0 to 38.95	*cF*4	$Fm\bar{3}m$
β	36.8 to 56.5	*cI*2	$Im\bar{3}m$
β´	45.5 to 50.7	*cP*2	$Pm\bar{3}m$
γ	57.7 to 70.6	*cI*52	$I\bar{4}3m$
δ	73.02 to 76.5	*hP*3	$P\bar{6}$
ε	78.5 to 88.3	*hP*2	$P6_3/mmc$
η or (Zn)	97.25 to 100	*hP*2	$P6_3/mmc$

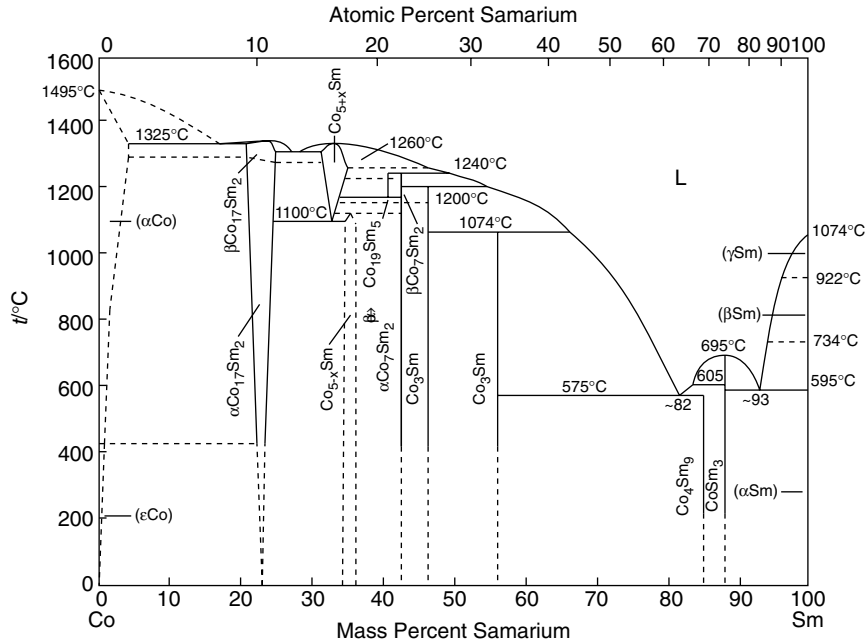

FIGURE 21. Co-Sm system.

Phase	Composition, mass % Sm	Pearson symbol	Space group
(αCo)	0 to ~3.7	*cF*4	$Fm\bar{3}m$
(εCo)	~0	*hP*2	$P6_3/mmc$
$\beta Co_{17}Sm_2$	~23.0	*hP*38	$P6_3/mmc$
$\alpha Co_{17}Sm_2$	~23.0	*hR*19	$R\bar{3}m$
		*hP*8	$P6/mmm$
$Co_{5+x}Sm$	~33 to 34	–	–
$Co_{5-x}Sm$	~34 to 35	–	–
$Co_{19}Sm_5$	~40.1	*hR*24	$R\bar{3}m$
		*hP*48	$P6_3/mmc$
αCo_7Sm_2	~42.1	*hR*18	$R\bar{3}m$
βCo_7Sm_2	~42.1	*hP*36	$P6_3/mmc$
Co_3Sm	46	*hR*12	$R\bar{3}m$
Co_2Sm	56.0	*hR*4	$R\bar{3}m$
		*cF*24	$Fd\bar{3}m$
Co_4Sm_9	~85.1	*o***	–
$CoSm_3$	88	*oP*16	*Pnma*
(γSm)	~100	*cI*2	$Im\bar{3}m$
(βSm)	~100	*hP*2	$P6_3/mmc$
(αSm)	~100	*hR*3	$R\bar{3}m$
Other reported phases			
Co_5Sm	~33.8	*hP*6	$P6/mmm$
Co_2Sm_5	~86.4	*mC*28	$C2/c$

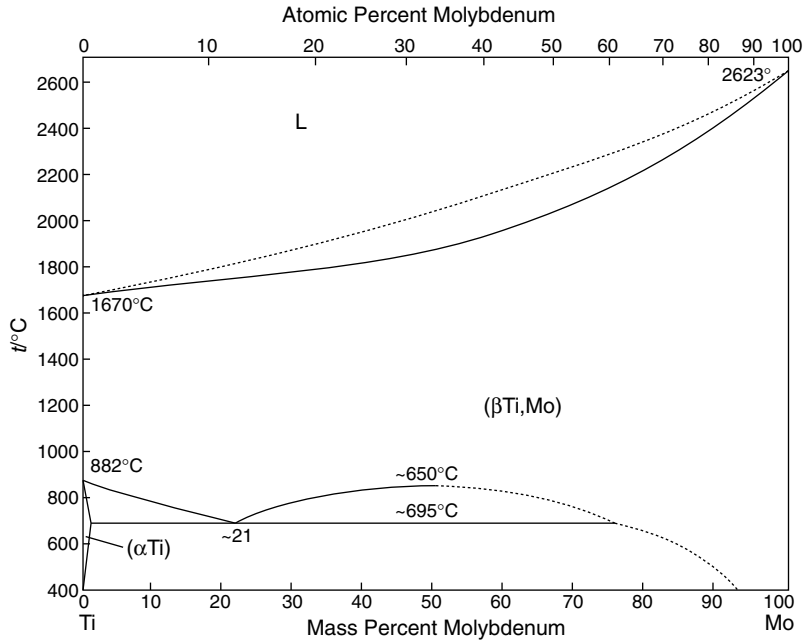

FIGURE 22. Ti-Mo system.

Phase	Composition, mass % Mo	Pearson symbol	Space group
(βTi, Mo)	0 to 100	*cI*2	$Im\bar{3}m$
(αTi)	0 to 0.8	*hP*2	$P6_3/mmc$
α′	(a)	*hP*2	$P6_3/mmc$
α″	(a)	*oC*4	*Cmcm*
ω	(a)	*hP*3	*P*6/*mmm*

(a) Metastable.

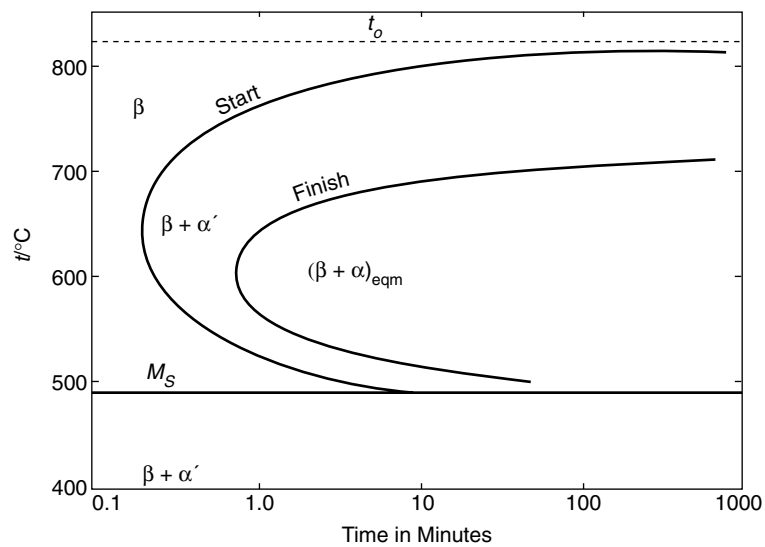

Experimental time-temperature-transformation (TTT) diagram for Ti-Mo. The start and finish times of the isothermal precipitation reaction vary with temperature as a result of the temperature dependence of the nucleation and growth processes. Precipitation is complete, at any temperature, when the equilibrium fraction of α is established in accordance with the lever rule. The solid horizontal line represents the athermal (or nonthermally activated) martensitic transformation that occurs when the β phase is quenched.

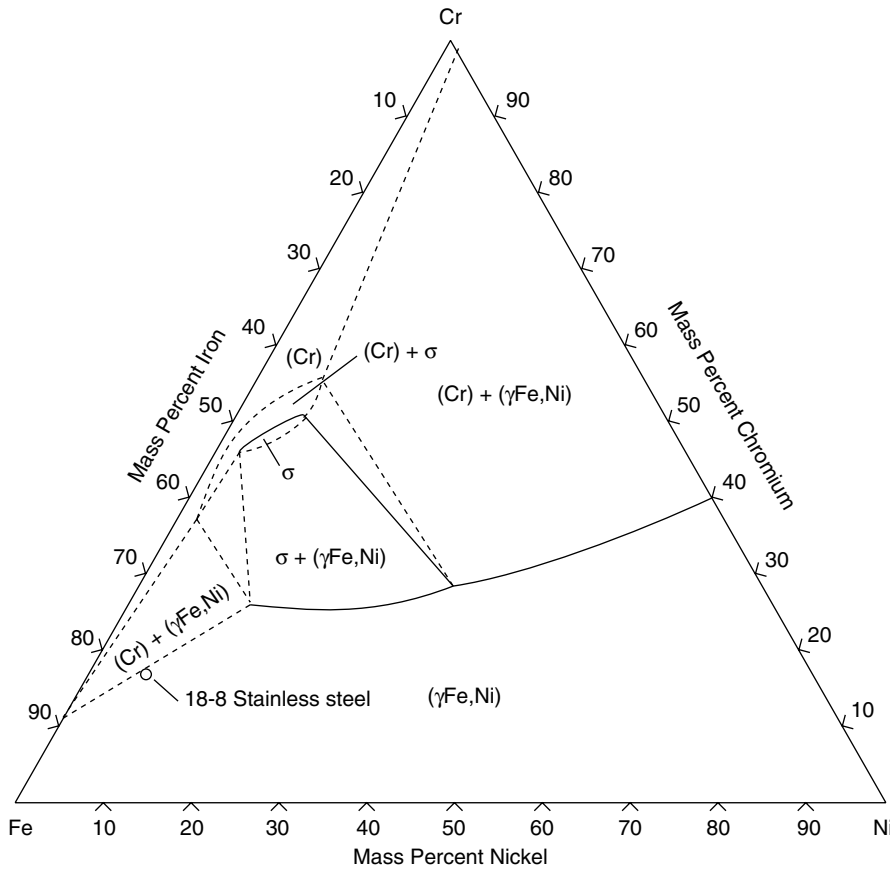

FIGURE 23. The isothermal section at 900°C (1652°F) of the iron-chromium-nickel ternary phase diagram, showing the nominal composition of 18-8 stainless steel.